XIX International Conference on Water Resources
CMWR 2012
University of Illinois at Urbana-Champaign
June 17-22,2012

AN UNFITTED METHOD FOR TWO-PHASE FLOW IN FRACTURED POROUS MEDIA

A. Fumagalli* **and A. Scotti***

* Politecnico di Milano
Department of Mathematics, MOX
Piazza Leonardo da Vinci 32, 20133 Milano, Italy.
e-mail: alessio.fumagalli@mail.polimi.it, anna.scotti@mail.polimi.it

Key words: Two-phase flow, reduced models, fractured porous media, XFEM

Summary. We propose an efficient computational method to simulate two-phase flow in fractured porous media. Instead of refining the grid to capture the flow along the faults or fractures, we represent them as immersed interfaces with reduced model for the flow and suitable coupling conditions. We allow for non matching grids between the porous matrix and the fracture to increase the flexibility of the method in realistic cases. We employ the extended finite element method for the Darcy problem and a finite volume method for the saturation equation, with a numerical flux that yields the correct entropy solution in the case of discontinuous flux function at the interface between the fracture and the porous matrix.

1 Introduction

It has been observed that fractures and faults can act as conduits or barriers for the flow. The effect of fractures on the flow is important in many different applications such as the study of fractured aquifers, geothermal fields, hydrocarbon reservoirs and unconventional sources. A relevant application that requires an accurate characterization of the faults from the geo-mechanical and hydrodynamic point of view is CO_2 storage, see [9]. At injection conditions, CO_2 is buoyant relative to the ambient groundwater, so it rises toward the top of the formation and, in the presence of a pre-existing well or fracture, or the activation of a fault, can leak into shallow formations. At basin scale the mesh refinement needed to capture the effect of faults and fractures, whose typical width is of the order of 1 meter, leads to an extremely high computational cost. One possibility to address this problem is to use a reduced model to represent the flow in fractures, represented as immersed interfaces coupled with the rest of the porous medium. A reduced model was first introduced by Alboin *et al.* , [1], and later extended by Martin *et al.* , [10] and Angot, [2]. In [5] this approach is further extended to allow for non-matching grids between the porous medium and the fracture thanks to the use of the extended finite element method

(XFEM). Removing the constraint of mesh conformity can be convenient in realistic cases with numerous and complex fractures. An advantage of a non-matching method is the possibility to run multiple simulations with different fractures configuration, in the case of uncertainty on geophysical parameters or multiple scenario analyses, without meshing the domain each time. In this paper we present an original numerical approximation strategy for two-phase flow in fractured media. We complement the Darcy problem, approximated as in [5], with a hyperbolic equation for the saturation of one of the two phases. We adapt the reduced model for two-phase flow presented in [8] to the case of negligible capillary effects and propose a finite volume scheme that is able to account for the matrix-fracture interaction and the cut elements in the non-conforming case. The faults and the porous matrix are characterized by different absolute and relative permeabilities, resulting in a flux function for the saturation equation which is discontinuous in space. Numerical schemes that yield the correct entropy solution in this case are required to obtain the physical solution. Some synthetic cases are presented to test the behaviour of the method with different configurations, *i.e.* in the presence of impermeable or open faults.

2 Mathematical model

We consider two distinct and immiscible fluid phases, denoted by the subscript $\alpha \in \{w, n\}$ for the wetting and non-wetting phase respectively, flowing in a highly heterogeneous porous medium crossed by fractures. The latter can be characterized by data, *e.g.* permeabilities, that differs significantly from the porous matrix. We neglect the effect of capillary pressure.

Let us consider a regular domain $\Omega \in \mathbb{R}^n$, $n = 2$ or 3, with boundary $\overline{\Gamma} = \overline{\Gamma}_N \cup \overline{\Gamma}_D$, $\Gamma_N \neq \emptyset$, and outward unit normal $\boldsymbol{n}_\Gamma$, cut by a thin region $\Omega_f \subset \Omega$ of thickness d representing the fracture. Let us set, from now on, $i \in \{1, 2, f\}$ and $j \in \{1, 2\}$. Figure 1 represents the partition $\overline{\Omega} = \bigcup_i \overline{\Omega}_i$ into three disjoint subsets of Ω. $\gamma_j \in \mathbb{R}^{n-1}$ is the interface between Ω_j and Ω_f with unit normal $\boldsymbol{n}_j$, pointing outwards with respect to Ω_j. We introduce

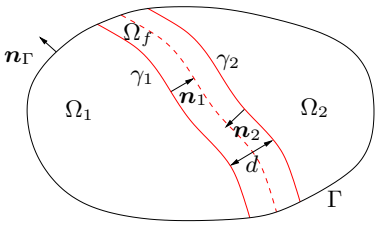

Figure 1: Sketch of Ω with the two sub-domains Ω_1 and Ω_2 divided by Ω_f.

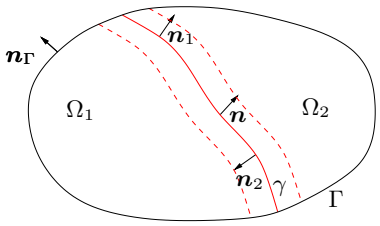

Figure 2: Sketch of Ω cut by the interface γ that replaces Ω_f.

the interval of time $\mathcal{I}_T := (0, T)$, divided into N subintervals $\mathcal{I}_T^m := (t^m, t^{m+1})$, with $\Delta t^m = |\mathcal{I}_T^m|$, such that $\overline{\mathcal{I}_T} = \bigcup_m \overline{\mathcal{I}_T^m}$ for $m \in \{0, \dots, N\}$. The space-time domains are thus defined as $Q_i := \Omega_i \times \mathcal{I}_T$. The two-phase system of equations in the *fractional flow formulation* [4, 8], which describes the evolution of the total velocity $\boldsymbol{u}$, the global pressure

p, the saturation of the non-wetting phase $S \in [0,1]$ and the velocity of the non-wetting phase $\boldsymbol{v}$, reads

$$\begin{cases} \nabla\cdot \boldsymbol{u}_i = 0 \\ \boldsymbol{u}_i = -\lambda_i \boldsymbol{K}_i \left(\nabla p_i - \boldsymbol{G}_i\right) \\ \Phi_i \dfrac{\partial S_i}{\partial t} + \nabla\cdot \boldsymbol{v}_i = 0 \\ \boldsymbol{v}_i = f_i \boldsymbol{u}_i + b_i \boldsymbol{K}_i \boldsymbol{g} \end{cases} \text{ in } Q_i, \text{ with } \begin{cases} \boldsymbol{u}_j \cdot \boldsymbol{n}_j = \boldsymbol{u}_f \cdot \boldsymbol{n}_j \\ p_j = p_f \\ \boldsymbol{v}_j \cdot \boldsymbol{n}_j = \boldsymbol{v}_f \cdot \boldsymbol{n}_j \end{cases} \text{ on } \gamma_j \times \mathcal{I}_T, \tag{1}$$

where the subscripts $_i$ and $_j$ denotes the restriction of the variables to Q_i or γ_j, respectively. Furthermore

$$\lambda_i := \frac{k_i^n}{\mu^n} + \frac{k_i^w}{\mu^w}, \quad \boldsymbol{G}_i := \frac{k_i^w \rho^w/\mu^w + k_i^n \rho^n/\mu^n}{\lambda_i} \boldsymbol{g}, \quad f_i := \frac{k_i^n}{\mu^n \lambda_i}, \quad b_i := \frac{k_i^n k_i^w}{\mu^n \mu^w \lambda_i} \left(\rho^n - \rho^w\right).$$

Here $\boldsymbol{K}_i$ denotes the absolute permeability tensor which is symmetric and positive definite and Φ_i is the porosity. For each phase α, k^α is the relative permeability, ρ^α the density and μ^α the dynamic viscosity. Finally $\boldsymbol{g}$ is the gravity acceleration vector. The relative permeabilities are non-linear functions of the saturation [3]. Using an *IMPES* type approach [4] to solve (1) we decouple the first two equations, called *pressure equations*, from the last two, called *saturation equations*, and we solve them in sequence at each time step $\mathcal{I}_T^m$. Hence the pressure equations, with fixed saturation S at $\mathcal{I}_T^m$, are

$$\begin{cases} \nabla \cdot \boldsymbol{u}_i = 0 \\ \boldsymbol{u}_i = -\lambda_i \boldsymbol{K}_i \left(\nabla p_i - \boldsymbol{G}_i\right) \end{cases} \text{ in } \Omega_i \times \mathcal{I}_T^{m+1}, \text{ with } \begin{cases} \boldsymbol{u}_j \cdot \boldsymbol{n}_j = \boldsymbol{u}_f \cdot \boldsymbol{n}_j \\ p_j = p_f \end{cases} \text{ on } \gamma_j \times \mathcal{I}_T^{m+1}. \tag{2}$$

We impose to (2) $p_i = \overline{p}_i$ on Γ_N and $\boldsymbol{u}_i \cdot \boldsymbol{n}_\Gamma = \overline{u}_i$ on Γ_D as boundary conditions. The saturation equations, with the computed total velocity $\boldsymbol{u}_i$ at time $\mathcal{I}_T^{m+1}$, read

$$\begin{cases} \Phi_i \dfrac{\partial S_i}{\partial t} + \nabla\cdot \boldsymbol{v}_i = 0 \\ \boldsymbol{v}_i = f_i \boldsymbol{u}_i + b_i \boldsymbol{K}_i \boldsymbol{g} \end{cases} \text{ in } \Omega_i \times \mathcal{I}_T^{m+1}, \text{ with } \boldsymbol{v}_j \cdot \boldsymbol{n}_j = \boldsymbol{v}_f \cdot \boldsymbol{n}_j \text{ on } \gamma_j \times \mathcal{I}_T^{m+1}. \tag{3}$$

We impose to (3) $S_i = \overline{S}_i$ on Γ_N and $\boldsymbol{v}_i \cdot \boldsymbol{n}_\Gamma = \overline{v}_i$ on Γ_D and $S_i = S_i^0$ in $\Omega_i \times \{0\}$ as the initial condition.

3 Reduced model for the two-phase flow

Following [8, 7], we present a reduced model for (2) and (3), replacing the region Ω_f with a $n-1$ dimensional interface $\gamma \approx \gamma_j$ with unit normal $\boldsymbol{n} \approx \boldsymbol{n}_1 \approx -\boldsymbol{n}_2$, as shown in Figure 2. We report the main results for readers convenience. Given a scalar or vector function $a : \Omega \to \mathbb{R}^q$, $q = 1$ or n, let us define

$$[\![a]\!]_\gamma := a_1 - a_2 \quad \text{and} \quad \{\!\{a\}\!\}_\gamma := \frac{a_1 + a_2}{2} \quad \text{with} \quad a_j(\boldsymbol{x}) := \lim_{\epsilon \to 0^\pm} a(\boldsymbol{x} - \epsilon \boldsymbol{n}).$$

We introduce the projection matrix $\boldsymbol{N} := \boldsymbol{n} \otimes \boldsymbol{n}$ so that, given $e : \Omega \to \mathbb{R}$ and $\boldsymbol{c} : \Omega \to \mathbb{R}^n$

$$\nabla_{\boldsymbol{\tau}} e := \nabla e - \boldsymbol{N}\nabla e \quad \text{and} \quad \nabla_{\boldsymbol{\tau}} \cdot \boldsymbol{c} := \nabla \cdot \boldsymbol{c} - \boldsymbol{N} : \nabla \boldsymbol{c}.$$

We indicate with $\hat{\cdot}$ the reduced variables defined on γ. The scalar unknowns $\hat{p}$ and $\hat{S}$ represent the averaged values across normal sections of Ω_f while the vector unknowns $\hat{\boldsymbol{u}}$ and $\hat{\boldsymbol{v}}$ are the tangential fluxes integrated over the normal sections of Ω_f. The properties of the fracture are averaged over each cross sections of Ω_f or assumed to be invariant in the normal direction. We assume that $\boldsymbol{K}_f = K_{f,\boldsymbol{n}}\boldsymbol{N} + K_{f,\boldsymbol{\tau}}(\boldsymbol{I} - \boldsymbol{N})$, and defining $\hat{\eta} := d/(\lambda_f K_{f,\boldsymbol{\tau}})$, equation (2) can be written as

$$\begin{cases} \nabla \cdot \boldsymbol{u}_j = 0 \\ \boldsymbol{u}_j = -\lambda_j \boldsymbol{K}_j (\nabla p_j - \boldsymbol{G}_j) \end{cases} \text{in } \Omega_j \times \mathcal{I}_T^{m+1}, \begin{cases} \nabla_{\boldsymbol{\tau}} \cdot \hat{\boldsymbol{u}} = [\![\boldsymbol{u} \cdot \boldsymbol{n}]\!]_\gamma \\ \hat{\eta}\hat{\boldsymbol{u}} + \nabla_{\boldsymbol{\tau}} \hat{p} = \hat{\boldsymbol{G}} \end{cases} \text{in } \gamma \times \mathcal{I}_T^{m+1}, \quad (4)$$

where $\hat{\boldsymbol{G}}$ is the tangential component of $\boldsymbol{G}$ integrated over each normal section of Ω_f. Introducing a shape parameter $\xi_0 \in (0, 0.25]$ and $\eta_\gamma := (d\lambda_f K_{f,\boldsymbol{n}})^{-1}$, the coupling conditions can be written as

$$\begin{cases} \xi_0 \eta_\gamma [\![\boldsymbol{u} \cdot \boldsymbol{n}]\!]_\gamma + \dfrac{d}{4} [\![\boldsymbol{G} \cdot \boldsymbol{n}]\!]_\gamma = \{\!\{p\}\!\}_\gamma - \hat{p} \\ \eta_\gamma \{\!\{\boldsymbol{u} \cdot \boldsymbol{n}\}\!\}_\gamma = [\![p]\!]_\gamma + d\{\!\{\boldsymbol{G} \cdot \boldsymbol{n}\}\!\}_\gamma \end{cases} \text{on } \gamma \times \mathcal{I}_T^{m+1}.$$

Similarly to (2) the reduced equations for (3) become

$$\begin{cases} \Phi_j \dfrac{\partial S_j}{\partial t} + \nabla \cdot \boldsymbol{v}_j = 0 \\ \boldsymbol{v}_j = f_j \boldsymbol{u}_j + b_j \boldsymbol{K}_j \boldsymbol{g} \end{cases} \text{in } \Omega_j \times \mathcal{I}_T^{m+1}, \begin{cases} d\Phi_f \dfrac{\partial \hat{S}}{\partial t} + \nabla_{\boldsymbol{\tau}} \cdot \hat{\boldsymbol{v}} = [\![\boldsymbol{v} \cdot \boldsymbol{n}]\!]_\gamma \\ \hat{\boldsymbol{v}} = f_f \hat{\boldsymbol{u}} + b_f K_{f,\boldsymbol{\tau}} \hat{\boldsymbol{g}} \end{cases} \text{in } \gamma \times \mathcal{I}_T^{m+1}, \quad (5)$$

where $\hat{\boldsymbol{g}}$ is the tangential component of $\boldsymbol{g}$ integrated over each normal section of Ω_f. The coupling condition becomes

$$\boldsymbol{v}_j(S_j) \cdot \boldsymbol{n}_j = \boldsymbol{v}_{f,j}(\hat{S}) \cdot \boldsymbol{n}_j \text{ on } \gamma, \text{ with } \boldsymbol{v}_{f,j}(\hat{S}) := f_f(\hat{S})\boldsymbol{u}_j + b_f(\hat{S}) K_{f,\boldsymbol{n}} \boldsymbol{N}\boldsymbol{g}.$$

4 Numerical approximation of the two-phase Darcy problem

The Darcy problem (2) is solved in mixed form, with the lowest order Raviart-Thomas finite elements enriched in the cut elements as proposed in [5, 6]. The choice of mixed finite elements guarantees a locally conservative velocity field for the subsequent solution of the saturation equation (3), which is carried out with the finite volumes method in the porous medium and in the fracture.

Let $\mathcal{T}_h$ be the triangulation of the domain Ω split into $\mathcal{T}_h = \mathcal{U}_h \cup \mathcal{C}_h$ with $\mathcal{U}_h$ the set of uncut elements and $\mathcal{C}_h$ the set of cut elements, and let $\hat{\mathcal{T}}_h$ be the mesh of the fracture. The approximate solution S_h, $\hat{S}_h$ for the saturation in the porous medium and in the fracture is sought in the following spaces

$$Q_h := Q_{1,h} \times Q_{2,h} \quad \text{with} \quad Q_{j,h} := \left\{ q_h \in L^2(\Omega_j) : \ q_h|_{K\cap\Omega_j} \in \mathbb{P}_0(K \cap \Omega_j), \ K \in \mathcal{T}_h \right\},$$
$$\hat{Q}_h := \left\{ \hat{q}_h \in L^2(\gamma) : \ \hat{q}_h|_{\hat{K}} \in \mathbb{P}_0\left(\hat{K}\right), \ \hat{K} \in \hat{\mathcal{T}}_h \right\}.$$

The finite volume approximation of (5) reads, in the case of uncut elements

$$\int_K \phi \frac{S_h^{m+1} - S_h^m}{\Delta t^m} dx + \int_{\partial K} \widetilde{\boldsymbol{v} \cdot \boldsymbol{n}_K}(S_h^m) ds = 0 \quad \text{for } K \in \mathcal{U}_h,$$

where $\widetilde{\boldsymbol{v} \cdot \boldsymbol{n}_K}$ is a suitable numerical flux and $\boldsymbol{n}_K$ is the outward unit normal to ∂K. In the cut elements the method has to be modified to account for the cut edges and for the presence of the fracture, yielding, for all $K \in \mathcal{C}_h$

$$\int_{K\cap\Omega_j} \phi \frac{S_h^{m+1} - S_h^m}{\Delta t^m} dx + \int_{\partial K\cap\Omega_j} \widetilde{\boldsymbol{v} \cdot \boldsymbol{n}_K}(S_h^m) ds + \int_{\gamma\cap K} (-1)^{j+1} \widetilde{\boldsymbol{v} \cdot \boldsymbol{n}}(S_h^m, \mathcal{M}(\hat{S}_h^m)) = 0,$$

where $\mathcal{M}(\hat{S}_h^m)$ is the interpolation of $\hat{S}_h^m$ on $\mathcal{T}_h$. The two meshes are indeed, in general, *genuinely* non matching as shown in Figure 3. The discrete problem in the fracture reads, for every $\hat{K} \in \hat{\mathcal{T}}_h$

$$\int_{\hat{K}} d\phi_f \frac{\hat{S}_h^{m+1} - \hat{S}_h^m}{\Delta t^m} dx + \int_{\partial \hat{K}} \widetilde{\hat{\boldsymbol{v}} \cdot \boldsymbol{n}_{\hat{K}}}(\hat{S}_h^m) ds - \sum_{j=1,2} \int_{\gamma\cap K} (-1)^{j+1} \mathcal{M}^*(\widetilde{\hat{\boldsymbol{v}} \cdot \boldsymbol{n}}(S_h^m, \mathcal{M}(\hat{S}_h^m))) = 0.$$

Here the operator $\mathcal{M}^*$ performs the interpolation from $\mathcal{T}_h$ to $\hat{\mathcal{T}}_h$. To obtain a conservative method we represent the operators $\mathcal{M}$ and $\mathcal{M}^*$ with a matrix and its transpose respectively.

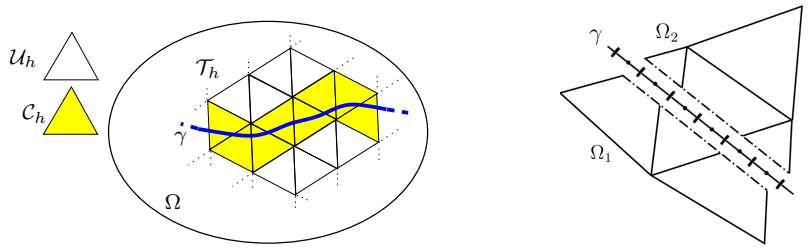

Figure 3: Sketch of $\mathcal{T}_h$ cut by γ. The mesh of γ is in general non-matching with the edges of the cut elements.

The choice of the numerical flux is critical in problems characterized, like the one of our interest, by a discontinuous flux function due to the presence of different rock types (typically the matrix and the fracture). We adopt the exact Godunov flux which, at the expense of a higher computational cost, satisfies the entropy condition and gives the physically correct solution, see [11] for further details.

5 Test Cases

We present two examples to highlight the potentiality and advantages of the proposed method. The first one deals with the effect of the fracture permeability and tests mass conservation for a flow driven only by gravity, while the second presents a coupled simulation with the IMPES splitting.

5.1 Flow driven by gravity

Let us consider a flow driven by gravity, *i.e.* $\boldsymbol{u}_j \equiv \hat{\boldsymbol{u}} \equiv 0$, in a square domain $\Omega = (0,1)^2$ cut by fracture $\gamma = \{(x,y) \in \Omega : y = -2x + 1.4\}$, where we set the initial saturation S_0 to 0.5 in the circle $(x-0.45)^2 + (y-0.15)^2 < 0.016$. The properties of the fluid and the media are reported in Table 5. In Figure 6 we compare three simulations characterized by

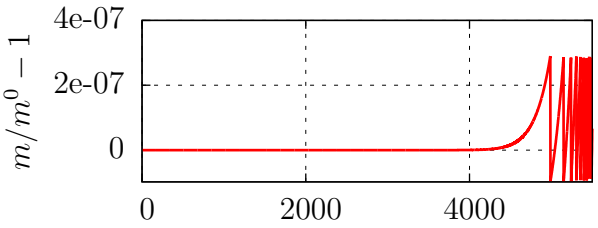

Figure 4: Plot of the conservation of mass over time steps. Here m is the global mass plus the outflow and with m^0 the global mass at initial time.

$k_i^n = 1 - S^2$	$k_i^w = S$
$\rho^w = 2$	$\rho^n = 1$
$\boldsymbol{g} = (0,-1)^\top$	$\mu^\alpha = 1$
$\Phi_i = 1$	$\boldsymbol{K}_j = \boldsymbol{I}$
$d = 0.01$	

Table 5: Data for the problem.

different types of fracture. In the first one the problem is solved without the fracture γ in the domain. We notice that the non-wetting fluid moves upwards due to buoyancy. In the second one we insert the fracture γ with the same absolute permeability of the medium. In this case the fracture acts as if it did not exists, indeed the result is very similar to the first simulation. Finally in the third one the fracture has the same normal permeability as the bulk, but the tangential permeability is twenty times higher. When the light fluid reaches γ the flow inside the fracture is faster and the saturation is transported upwards more rapidly.
We verified numerically that the method is conservative. The graph in Figure 4 compares, for the third simulation, the mass present in the domain and the cumulative outflow with the initial mass m_0. We see a perfect conservation of mass until the outflow boundary is reached, *i.e.* after ~ 4000 time steps. From that time on there are only very small oscillations of about $10^{-5}\%$.

5.2 Fully coupled two-phase flow

In this example we consider the complete two-phase flow model (4) and (5) in an horizontal plane, *i.e.* without gravity. We set as the initial condition $S_0 = 1$ in the circle $(x-0.45)^2 +$

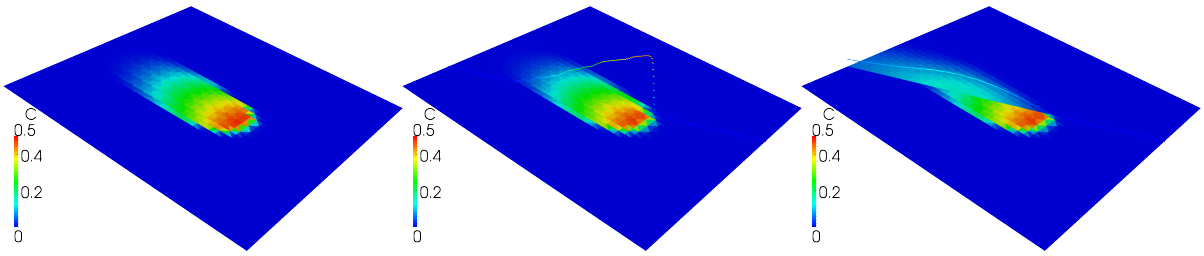

Figure 6: Snapshots of the solution at $t \simeq 1$ in three different cases: on the left S_h without fractures, in the centre S_h and $\hat{S}_h$ with γ whose properties are equal to the bulk medium and on the right with γ more conductive in the tangential direction. Here $\hat{S}_h$ is warped for the sake of visualization.

$(y - 0.15)^2 < 0.016$. The permeabilities in the fracture are $K_{f,\boldsymbol{\tau}} = 1$ and $K_{f,\boldsymbol{n}} = 10^{-3}$ while the rest of the data are the same as in the previous test case, see Table 5.

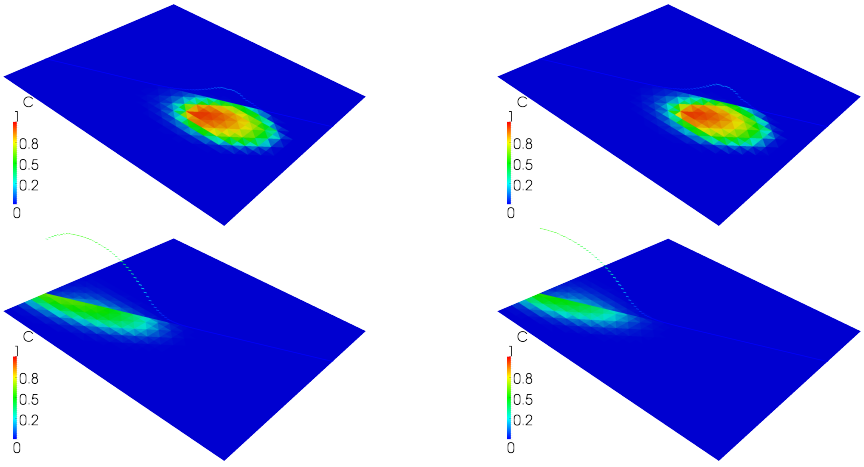

Figure 7: Comparison of S_h and $\hat{S}_h$ for the two strategies: on the left with a constant velocity and on the right the coupled problem. On the top the solution at $t \simeq 0.27$ and on the bottom at $t \simeq 1.1$.

Figure 7 compares the evolution of saturation obtained with a constant velocity field with the result of the fully coupled two-phase problem. We notice that even if the solutions look similar in the beginning the real velocity field changes in time and after some time the difference between the two solutions becomes more noticeable.

6 Conclusions

Future works should focus on the extension of the method to cases with more complex geometries (multiple and intersecting fractures) and realistic values of the parameters, as well as on the inclusion of the capillary term. In both the examples we presented the CFL condition turned out to be a severe constraint the presence of small sub-elements in the cut region of the mesh: suitable numerical techniques to overcome this limitation will be the subject of future study.

REFERENCES

[1] Clarisse Alboin, Jérôme Jaffré, Jean E. Roberts, Xuewen Wang, and Christophe Serres. *Domain decomposition for some transmission problems in flow in porous media*, volume 552 of *Lecture Notes in Phys.*, pages 22–34. Springer, Berlin, 2000.

[2] Philippe Angot, Franck Boyer, and Florence Hubert. Asymptotic and numerical modelling of flows in fractured porous media. *M2AN Math. Model. Numer. Anal.*, 43(2):239–275, 2009.

[3] Jacob Bear. *Dynamics of Fluids in Porous Media*. American Elsevier, 1972.

[4] Guy Chavent and Jérôme Jaffré. *Mathematical Models and Finite Elements for Reservoir Simulation*, volume 17. Elsevier, 1986.

[5] Carlo D'Angelo and Anna Scotti. A Mixed Finite Element Method for Darcy Flow in Fractured Porous Media with Non-Matching Grids. *Mathematical Modelling and Numerical Analysis*, 2011.

[6] Alessio Fumagalli and Anna Scotti. Numerical modelling of multiphase subsurface flow in the presence of fractures. *Communications in Applied and Industrial Mathematics*, 2011.

[7] Alessio Fumagalli and Anna Scotti. A reduced model for flow and transport in fractured porous media with non-matching grids. Technical Report 03/2012, Politecnico di Milano, 2012.

[8] J. Jaffré, M. Mnejja, and J.E. Roberts. A discrete fracture model for two-phase flow with matrix-fracture interaction. *Procedia Computer Science*, 4:967–973, 2011.

[9] C. W. MacMinn, M. L. Szulczewski, and R. Juanes. CO_2 migration in saline aquifers. Part 1. Capillary trapping under slope and groundwater flow. *J. Fluid Mech.*, 662:329–351, 2010.

[10] Vincent Martin, Jérôme Jaffré, and Jean E. Roberts. Modeling fractures and barriers as interfaces for flow in porous media. *SIAM J. Sci. Comput.*, 26(5):1667–1691 (electronic), 2005.

[11] Siddhartha Mishra and Jérôme Jaffré. On the upstream mobility scheme for two-phase flow in porous media. *Comput. Geosci.*, 14(1):105–124, 2010.